

M acetic acid to remove diagenetic carbonates. The samples were freeze-dried and placed into individual reaction vessels in a Kiel II aut carbonate device. They were reacted with phosphoric acid at 70°C, and clean dry CO₂ was obtained by cryogenic distillation. ¹³C/¹²C ratios were measured on a Finnigan MAT 252 mass spectrometer with a precision of ±0.1‰.

28. C₃ signatures indicate that these herbivores were browsers or browser/frugivores, because there is no evidence of C₃ grasses (as evidenced by grazer δ¹³C values) at Makapansgat.

29. R. S. O. Harding, *Folia Primatol.* **25**, 143 (1976).

30. R. I. M. Dunbar and U. Bose, *Primates* **32**, 1 (1991).

31. K. R. L. Hall, *J. Zool.* **148**, 15 (1965).

32. H. Kummer, *Social Organization of Hamadryas Baboons* (Univ. of Chicago Press, Chicago, IL, 1968).

33. R. J. Clarke and P. V. Tobias, *Science* **269**, 521 (1995).

34. H. M. McHenry and L. R. Berger, *J. Hum. Evol.* **35**, 1 (1998).

35. M. F. Teaford, in *Theropithecus: the Rise and Fall of a Primate Genus*, N. Jablonski, Ed. (Cambridge Univ. Press, Cambridge, 1992), pp. 331–349.

36. T. D. White, D. C. Johanson, W. H. Kimbel, *S. Afr. J. Sci.* **77**, 445 (1981).

37. W. C. McGrew, *Chimpanzee Material Culture: Implications for Human Evolution* (Cambridge Univ. Press, Cambridge, 1992).

38. A. Walker, R. E. Leakey, J. M. Harris, F. H. Brown, *Nature* **322**, 517 (1986).

39. W. R. Leonard and M. L. Robertson, *Am. J. Hum. Biol.* **6**, 77 (1994).

40. L. C. Aiello and P. Wheeler, *Curr. Anthropol.* **36**, 199 (1995).

41. W. H. Kimbel *et al.*, *J. Hum. Evol.* **31**, 549 (1996).

42. S. Semaw *et al.*, *Nature* **385**, 333 (1997).

43. A. Sillen, G. Hall, R. Armstrong, *J. Hum. Evol.* **28**, 277 (1995).

44. J. A. Lee-Thorp, unpublished material.

45. K. D. Schick and N. Toth, *Making Silent Stones Speak* (Simon and Schuster, New York, 1993).

46. We thank S. Ambrose, L. Berger, R. Blumenschine, S. Cachel, R. Clarke, C. Feibel, C. Gow, J. Harris, T. Hoffman, P. Koch, Y. Lam, J. Lanham, D. Lieberman, C. Lockwood, J. Moggi-Cecchi, R. Palumbit, J. Parkington, S. Pfeiffer, M. Raath, Y. Rahman, K. Reed, B. Rubidge, C. Schrire, J. Sealy, S. Semaw, A. Sillen, J. Tactikos, P. Tobias, P. Ungar, and N. van der Merwe. This research was funded by NSF, the Foundation for Research Development, the Leakey Foundation, the Wenner-Gren Foundation, the Boise Fund, Rutgers University, and the University of Cape Town.

9 September 1998; accepted 18 November 1998

Ozone Isotope Enrichment: Isotopomer-Specific Rate Coefficients

K. Mauersberger,* B. Erbacher, D. Krankowsky, J. Günther, R. Nickel

Six rate coefficients of relative ozone formation contradict the role of molecular symmetry in the process that results in the enrichment of heavy ozone isotopomers. The results show that collisions between light atoms, such as ¹⁶O, and heavy molecules, such as ³⁴O₂ and ³⁶O₂, have a rate coefficient advantage of about 25 and 50 percent, respectively, over collisions involving heavy atoms and light molecules. These results suggest that the observed isotope effect for each isotopomer may be caused by the preponderance of a single reaction channel and not through molecular symmetry selection.

A problem in molecular and atmospheric physics has puzzled scientists for almost two decades: the unusually high enrichment in most of the heavy isotopomers of ozone (1). This isotope effect has been observed in tropospheric (2) and stratospheric (3) ozone and has been studied in detail in numerous laboratory experiments (4). Despite the progress that has been made during the past 10 years, a convincing physical explanation of the process that results in enrichment is still missing. Ozone is perhaps the most important trace gas in the atmosphere, and its isotope effect is not only an unresolved problem in molecular physics but is also of importance for atmospheric chemistry (5).

Laboratory production of ozone in atmospheric oxygen (6) permits the determination of isotopomers ⁴⁸O₃, ⁴⁹O₃, and ⁵⁰O₃, where ¹⁷O is substituted in the second molecule and ¹⁸O is substituted in the third molecule of these isotopomers. After the discovery of an almost equal enrichment (7) in the two heavy ozone molecules, which cannot be understood as a conventional isotope effect, a symmetry-selective pro-

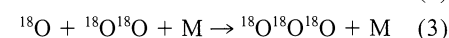
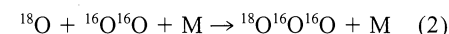
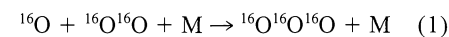
cess in the formation reaction was suggested (8). For ozone species ⁴⁹O₃ and ⁵⁰O₃, about one-third of all molecules are symmetric (for example, ¹⁶O¹⁸O¹⁶O), and two-thirds are asymmetric (for example, ¹⁶O¹⁶O¹⁸O); it was proposed (8) that the asymmetric reaction intermediate in the O + O₂ collision has a longer lifetime than the symmetric reaction intermediate, which results in an efficient quenching to ground state ozone [a proposal that was not confirmed by experiments (4)].

An apparent role of symmetry was found again when the distribution of all ozone isotopomers was measured (Fig. 1). A slight depletion of heavy symmetric molecules ¹⁷O¹⁷O¹⁷O and ¹⁸O¹⁸O¹⁸O was observed, whereas the highest enhancement (~18%) was measured in the isotopic combination ¹⁶O¹⁷O¹⁸O, which is an isotopomer with a mass of 51 atomic mass units (amu) and is composed exclusively of asymmetric molecules. All other isotope fractionations are about one-third less. Because of this, Anderson *et al.* (9) proposed a mechanism in which, during the ozone formation process, symmetry-selective relaxation from low-lying electronic metastable states to the ground state occurs. Metastable states have indeed been found (10), but a connection to the isotope effect has not been made to date.

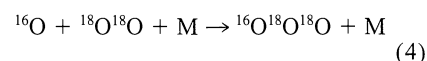
Gellene (11) recently modeled the isotope

fractionation shown in Fig. 1 based on nuclear symmetry. In his approach, symmetry restrictions arise for homonuclear diatomics (for example, ¹⁶O¹⁶O and ¹⁸O¹⁸O) involved in the O + O₂ collision because a fraction of their rotational states (*f* parity) correlate with those of the corresponding ozone molecule. In contrast, in the case of heteronuclear oxygen molecules (for example, ¹⁶O¹⁸O), all of their rotational states (*e* and *f* parity) correlate with those of the resulting ozone molecule. Gellene's theory can reproduce the general features of the enrichment pattern quite well. A number of other attempts have been made (12) to find an explanation for the isotope anomaly; none were able to account for the experimental results (4).

The role of molecular symmetry was questioned by Anderson *et al.* (13), who presented rate coefficients of four selected ozone formation channels. Whereas three channels



had similar rates of formation, which were consistent with a value of ~6 × 10⁻³⁴ cm⁶ s⁻¹, the fourth reaction channel



resulted in a rate coefficient that was 50% higher than the other three; M represents a third-body molecule. The difference in the rate coefficients of reactions 2 and 4 was unexpected. As seen in Fig. 1, molecules with masses of 50 and 52 amu that were substituted with ¹⁸O show similar isotope enrichments of ~13.0 and 14.4%, respectively (14). Reactions 2 and 4 produce mainly asymmetric molecules (with the colliding atom becoming the end member of the ozone molecule) (15). Thus, the difference in the rate coefficients of reactions 2 and 4 does not support an important role of symmetry in the isotope enrichment process. A similar conclusion was reached by Sehested *et al.* (16), who performed rate coefficient studies for the ¹⁶O-¹⁸O system on dual-channel processes, using CO₂ and Ar as third-body molecules, but

Max-Planck-Institut für Kernphysik, Division of Atmospheric Physics, P.O. Box 103 980, D-69029 Heidelberg, Germany.

*To whom correspondence should be addressed.

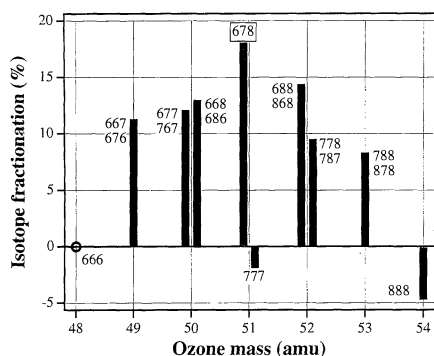


Fig. 1. Measured enrichment or depletion of all possible ozone isotopes (7, 14). Labels 6, 7, and 8 stand for ^{16}O , ^{17}O , and ^{18}O , respectively. Ozone was produced in two isotopically enriched oxygen mixtures of well-known composition at 70 torr and room temperature. The statistical abundance of each isotope was calculated and used to derive the isotopic fractionation from the measured values. The values in the graph are normalized so that $^{48}\text{O}_3$ has zero enrichment. Figure 1 is reproduced from work by Krankowsky and Mauersberger (7).

without isolating the process contributing to the enrichments.

Here, we report the experimental results of single-channel ozone recombination reactions involving the ^{17}O isotope. Using gas mixtures that were highly enriched in $^{17}\text{O}^{17}\text{O}$, we considerably increased the number of processes studied. The experimental technique has been somewhat altered and simplified in comparison with the earlier absolute measurements (13). Relative rate coefficients were determined to eliminate the necessity of knowing the atomic concentration in the gas in which ozone is formed.

The experimental procedure can be summarized as follows. With a mixture of two molecular oxygen gases (for example, $^{32}\text{O}_2$ and $^{36}\text{O}_2$) that are pure, nonscrambled, and at 20 torr each (with N_2 added to create a total pressure of 200 torr), ultraviolet photolysis produced atomic oxygen species that reacted with molecular oxygen to form four ozone isotopomers ($^{48}\text{O}_3$, $^{50}\text{O}_3$, $^{52}\text{O}_3$, and $^{54}\text{O}_3$), as shown in reactions 1 through 4. Other mixtures of $^{34}\text{O}_2$ and $^{32}\text{O}_2$, as well as mixtures of $^{34}\text{O}_2$ and $^{36}\text{O}_2$, enabled the

Table 1. Relative rate coefficients of six ozone formation channels. References are the three homonuclear ozone recombination rates resulting in $^{48}\text{O}_3$, $^{51}\text{O}_3$, and $^{54}\text{O}_3$. To a first approximation, their formation rates can be considered as equal.

Reaction	Relative rate coefficient
$^{16}\text{O} + ^{36}\text{O}_2 / ^{16}\text{O} + ^{32}\text{O}_2$	1.53 ± 0.03
$^{18}\text{O} + ^{32}\text{O}_2 / ^{18}\text{O} + ^{36}\text{O}_2$	0.90 ± 0.03
$^{16}\text{O} + ^{34}\text{O}_2 / ^{16}\text{O} + ^{32}\text{O}_2$	1.23 ± 0.03
$^{17}\text{O} + ^{32}\text{O}_2 / ^{17}\text{O} + ^{34}\text{O}_2$	1.01 ± 0.05
$^{18}\text{O} + ^{34}\text{O}_2 / ^{18}\text{O} + ^{36}\text{O}_2$	1.00 ± 0.06
$^{17}\text{O} + ^{36}\text{O}_2 / ^{17}\text{O} + ^{34}\text{O}_2$	1.29 ± 0.07

Table 2. Measured and derived rate coefficients for ozone formation processes. The rate coefficients are relative to the standard rate for $^{16}\text{O} + ^{32}\text{O}_2 + \text{M}$ of $6.05 \times 10^{-34} \text{ cm}^6 \text{ s}^{-1}$ (20). Derived rate coefficients are the sum of the reaction that results in a symmetric molecule and the reaction that results in an asymmetric molecule, which has been omitted for clarity. The enrichments (in percent) are also displayed in Fig. 1. Dashes, not applicable.

Isotope mass	Enrichment mass spectrometric (%)	Measured rate coefficient		Derived rate coefficient	
		Reaction	Value	Reaction	Value
48	0.0	$^{16}\text{O} + ^{16}\text{O}^{16}\text{O}$	1.00	—	—
49	11.3	$^{17}\text{O} + ^{16}\text{O}^{16}\text{O}$	1.03	$^{16}\text{O} + ^{17}\text{O}^{16}\text{O}$	1.17
50	13.0	$^{18}\text{O} + ^{16}\text{O}^{16}\text{O}$	0.93	$^{16}\text{O} + ^{18}\text{O}^{16}\text{O}$	1.27
50	12.1	$^{16}\text{O} + ^{17}\text{O}^{17}\text{O}$	1.23	$^{17}\text{O} + ^{16}\text{O}^{17}\text{O}$	1.11
51	-1.8	$^{17}\text{O} + ^{17}\text{O}^{17}\text{O}$	—	$^{17}\text{O} + ^{17}\text{O}^{17}\text{O}$	1.02
52	14.4	$^{16}\text{O} + ^{18}\text{O}^{18}\text{O}$	1.53	$^{18}\text{O} + ^{16}\text{O}^{18}\text{O}$	1.01
52	9.5	$^{18}\text{O} + ^{17}\text{O}^{17}\text{O}$	1.03	$^{17}\text{O} + ^{18}\text{O}^{17}\text{O}$	1.21
53	8.3	$^{17}\text{O} + ^{18}\text{O}^{18}\text{O}$	1.31	$^{18}\text{O} + ^{17}\text{O}^{18}\text{O}$	1.09
54	-4.6	$^{18}\text{O} + ^{18}\text{O}^{18}\text{O}$	1.03	—	—

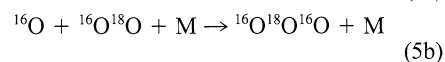
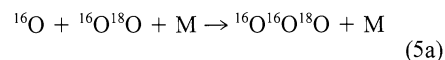
study of different reaction channels. The fast isotope exchange reaction (13, 17) between oxygen molecules and atoms kept atomic oxygen in isotopic equilibrium with molecular oxygen in the reaction cell; that is, atomic oxygen essentially maintained the isotopic composition of the molecular bath gas. However, heteronuclear species such as $^{16}\text{O}^{18}\text{O}$ or $^{17}\text{O}^{18}\text{O}$ formed rapidly. Therefore, photolysis times had to be kept short (typically <2 min) to ensure a small amount of ozone formation (a few percent) through heteronuclear channels. A mass spectrometer molecular beam system (18) monitored the development of the gas composition in the cell. The relative rate coefficient of reaction channels involving the same atomic oxygen species were directly calculated from the ratio of mass peak intensities and the ratios of molecular oxygen concentrations. The final data analysis included corrections for ozone channels that resulted from impurities (particularly from newly formed heteronuclear oxygen species).

The high rate coefficient for reaction 4 that was previously found (13) has been confirmed and is given as a ratio of 1.53 (relative to $^{48}\text{O}_3$) (Table 1). Reaction 2 shows a value that is below that of $^{18}\text{O} + ^{36}\text{O}_2$. The four new relative rate coefficients involving ^{17}O provided the necessary information to investigate the surprising rate coefficient advantage of reaction 4: The relative rate coefficients for the two reactions involving light isotopes in the molecule and heavy atomic oxygen are close to 1, whereas the relative rate coefficients for the other two reactions where the positions of light and heavy isotopes are reversed are 23 and 29% higher, respectively.

Two immediate observations can be made. First, molecular symmetry cannot explain the ozone isotope enhancement process. All six reactions (relative to a homonuclear ozone molecule) produce asymmetric molecules. Therefore, if molecular symmetry was the driving

factor, the rate of formation of asymmetric molecules should be about equal to and higher than the rates for homonuclear ozone. Similarly, Gellene's theory of nuclear symmetry-induced kinetic isotope effects (11) cannot explain the observed variation of the formation rate coefficients. His model predicts a rate coefficient advantage of up to a factor of 2 when the oxygen molecule reactant is heteronuclear. Second, a rule can be derived for the rate coefficient advantage that is apparent in the data shown in Table 1: A collision between a light oxygen atom and a heavier molecule will result in a rate coefficient that is higher than the coefficient from reactions involving only one isotope, whereas collisions between heavier atoms with lighter molecules will not. The reaction of the lightest atom (^{16}O) with the heaviest molecule ($^{36}\text{O}_2$) clearly has the fastest rate. The rate coefficient advantage of $^{16}\text{O} + ^{34}\text{O}_2 / ^{16}\text{O} + ^{32}\text{O}_2$ in Table 1, where $^{36}\text{O}_2$ has been replaced by $^{34}\text{O}_2$, is about half that of $^{16}\text{O} + ^{36}\text{O}_2 / ^{16}\text{O} + ^{32}\text{O}_2$. The slowest reaction is $^{18}\text{O} + ^{32}\text{O}_2 / ^{18}\text{O} + ^{36}\text{O}_2$, with the atom being the heaviest in relation to the molecule, and $^{17}\text{O} + ^{36}\text{O}_2 / ^{17}\text{O} + ^{34}\text{O}_2$ is of the same kind as $^{16}\text{O} + ^{34}\text{O}_2 / ^{16}\text{O} + ^{32}\text{O}_2$.

The absolute and relative rate coefficients for ozone isotopomer formation are casting new light on past mass spectrometric isotope studies (Fig. 1). Those studies were all performed in scrambled oxygen mixtures, and during photolysis or electric discharge of molecular oxygen, more than one process contributed to the formation of an ozone isotopomer of a specific mass. For example, $^{50}\text{O}_3$ in atmospheric oxygen is formed almost exclusively through reaction 2 and the following processes:



From the data presented in Table 1, it is clear that reaction 2 cannot contribute to the en-

richments of 13% (Fig. 1) and may actually result in a slight depletion. Consequently, reactions 5a and 5b must be responsible for the enrichment. A tunable diode laser experiment (19) revealed that the symmetric molecule formed in reaction 5b may contribute only 10% to the enrichment, and therefore reaction 5a must carry a large rate coefficient advantage of ~43% to account for the mass spectrometric observations.

More detailed conclusions from the relative rate coefficients that are shown in Table 1 can only be drawn when the values of the three homonuclear reaction rates for ozone are known. Using the absolute values for $^{16}\text{O} + ^{32}\text{O}_2$ and $^{18}\text{O} + ^{36}\text{O}_2$ that were derived by Anderson *et al.* (20), we inferred by interpolation that the rate coefficient for $^{17}\text{O} + ^{34}\text{O}_2$ is $6.15 \times 10^{-34} \text{ cm}^6 \text{ s}^{-1}$ (21). The missing rates contributing to a specific isotope can now be calculated from the total enrichments measured in scrambled oxygen mixtures (Fig. 1). The derived rate coefficient ratios in Table 2 represent the sum of the symmetric and asymmetric reaction channels, which may be separated in future tunable diode laser experiments. The rule derived for atomic oxygen collisions also holds for reactions with heteronuclear species: ^{16}O collisions result in a higher rate of formation, whereas collisions with ^{18}O are close to the formation rate of the reaction $^{16}\text{O} + ^{32}\text{O}_2$. Reaction $^{16}\text{O} + ^{18}\text{O}^{16}\text{O}$ is the fastest, $^{16}\text{O} + ^{17}\text{O}^{16}\text{O}$ and $^{17}\text{O} + ^{18}\text{O}^{17}\text{O}$ are similar but slower, $^{17}\text{O} + ^{16}\text{O}^{17}\text{O}$ and $^{18}\text{O} + ^{17}\text{O}^{18}\text{O}$ are even slower, and $^{18}\text{O} + ^{16}\text{O}^{18}\text{O}$ is the slowest.

The results presented here provide new insights into the puzzling ozone isotope effect. It is not the symmetry of a molecule that determines the magnitude of the enrichment, but rather it is the nature of the collision process that occurs when ozone is produced in a nitrogen-oxygen gas mixture.

References and Notes

- D. Krankowsky and K. Mauersberger, *Science* **274**, 1324 (1996).
- D. Krankowsky *et al.*, *Geophys. Res. Lett.* **22**, 1713 (1995); J. C. Johnston and M. H. Thiemens, *J. Geophys. Res.* **102**, 25395 (1997).
- A summary of stratospheric $^{50}\text{O}_3$ enrichments results can be found in work by F. W. Irion *et al.*, *Geophys. Res. Lett.* **23**, 2377 (1996).
- M. H. Thiemens and T. Jackson, *ibid.* **15**, 639 (1988); *ibid.* **17**, 717 (1990); J. Morton, J. Barnes, B. Schueler, K. Mauersberger, *J. Geophys. Res.* **95**, 901 (1990).
- Y. L. Yung *et al.*, *J. Geophys. Res.* **102**, 10857 (1997).
- The isotope composition of atmospheric oxygen is [^{16}O] = 99.756%, [^{17}O] = 0.038%, and [^{18}O] = 0.205% throughout the troposphere and stratosphere.
- The enrichments listed in percent are calculated with the expression $E(\%) = [(^{16}\text{O}_3/^{48}\text{O}_3)_{\text{meas}} / (^{16}\text{O}_3/^{48}\text{O}_3)_{\text{calc}} - 1] \times 100\%$ with mass $M = 49$ through 54. For ozone produced in atmospheric oxygen, we used the values listed in (6) to calculate the statistical ratios.
- J. E. Heidenreich III and M. H. Thiemens, *J. Chem. Phys.* **84**, 2129 (1986).
- S. M. Anderson *et al.*, *ACS Symp. Ser.* **502**, 155 (1992).
- S. M. Anderson and K. Mauersberger, *J. Geophys. Res.* **100**, 3033 (1995); D. W. Arnold, C. Xu, E. H. Kim, D. M. Neumark, *J. Chem. Phys.* **101**, 912 (1994).
- G. I. Gellene, *Science* **274**, 1344 (1996).
- J. J. Valentini, *J. Chem. Phys.* **86**, 6757 (1987); D. R. Bates, *Geophys. Res. Lett.* **15**, 13 (1988); W. L. Morgan and D. R. Bates, *Planet. Space Sci.* **40**, 1573 (1992); K. S. Griffith and G. I. Gellene, *J. Chem. Phys.* **96**, 4403 (1992).
- S. M. Anderson, D. Hülsebusch, K. Mauersberger, *J. Chem. Phys.* **107**, 5385 (1997).
- K. Mauersberger, J. Morton, B. Schueler, J. Stehr, S. M. Anderson, *Geophys. Res. Lett.* **20**, 1031, 1993.
- N. W. Larsen, T. Pedersen, J. Sehested, *Int. J. Chem. Kinet.* **23**, 331 (1991).
- J. Sehested, O. J. Nielsen, H. Egsgaard, *J. Geophys. Res.* **100**, 20979 (1995); *ibid.* **103**, 3545 (1998).
- J. A. Kaye and D. F. Strobel, *ibid.* **88**, 8447 (1983).
- K. Mauersberger, *Rev. Sci. Instrum.* **48**, 1169 (1977).
- S. M. Anderson, J. Morton, K. Mauersberger, *Chem. Phys. Lett.* **156**, 175 (1989).
- The actual values found by Anderson *et al.* (13) are $^{16}\text{O} + ^{32}\text{O}_2 + \text{M} = 6.05 \times 10^{-34} \text{ cm}^6 \text{ s}^{-1}$, $^{18}\text{O} + ^{36}\text{O}_2 + \text{M} = 6.25 \times 10^{-34} \text{ cm}^6 \text{ s}^{-1}$, $^{18}\text{O} + ^{32}\text{O}_2 + \text{M} = 6.26 \times 10^{-34} \text{ cm}^6 \text{ s}^{-1}$, and $^{16}\text{O} + ^{36}\text{O}_2 + \text{M} = 8.98 \times 10^{-34} \text{ cm}^6 \text{ s}^{-1}$. A ratio for the isotope exchange reaction rates $k_{18\text{O}}/k_{16\text{O}} = 1.245$ was used; this ratio is in agreement with the experimental data presented in (13) and in Fig. 1.
- The purity of the available ^{17}O gas was not sufficiently high to obtain an absolute rate coefficient that was comparable in accuracy to $^{16}\text{O} + ^{32}\text{O}_2$ and $^{18}\text{O} + ^{36}\text{O}_2$.
- We thank S. M. Anderson at Augsburg College, who contributed substantially to the experiment and obtained the first set of rate coefficients.

14 September 1998; accepted 1 December 1998

Self-Assembly of Ordered Microporous Materials from Rod-Coil Block Copolymers

Samson A. Jenekhe* and X. Linda Chen

Rod-coil diblock copolymers in a selective solvent for the coil-like polymer self-organize into hollow spherical micelles having diameters of a few micrometers. Long-range, close-packed self-ordering of the micelles produced highly iridescent periodic microporous materials. Solution-cast micellar films consisted of multilayers of hexagonally ordered arrays of spherical holes whose diameter, periodicity, and wall thickness depended on copolymer molecular weight and composition. Addition of fullerenes into the copolymer solutions also regulated the microstructure and optical properties of the microporous films. These results demonstrate the potential of hierarchical self-assembly of macromolecular components for engineering complex two- and three-dimensional periodic and functional mesostructures.

Ordered mesoporous solids with nanoscale pore sizes are of interest in areas such as catalysis, sensors, size- and shape-selective separation media, adsorbents, and scaffolds for composite materials synthesis (1, 2). Those with pore sizes on the order of 50 nm to 10 μm are also of interest for applications in photonics, optoelectronics, lightweight structural materials, and thermal insulation (2–5). Most current general methods for preparing diverse porous materials use self-organized surfactants, block copolymers, or colloidal particles as templates in conjunction with sol-gel techniques (1–3). In these methods, the organic templates are eventually removed by thermal decomposition or solvent extraction to achieve the porous solid. Recently reported hollow spherical micelles of rod-coil diblock copolymers (6) represent a previously unknown class of colloidal particles (7). Their self-organization into long-range crystalline order could open the way to novel colloidal crys-

tals (8, 9), unusual microgels, and direct self-assembly of ordered microporous materials.

Polymer latex and silica spheres are known to form colloidal crystals (8, 9), but long-range ordering of suspensions of block copolymer micelles into body-centered cubic (bcc) and face-centered cubic (fcc) lattices was observed and elucidated more recently (10). Micelles of coil-coil block copolymers in a selective solvent for one of the blocks are spheres consisting of a dense core of the insoluble block and a diffuse corona of the solvated block (10–12). Copolymer architecture and solution chemistry have been used to vary their diameter between about 10 and 80 nm and the corona thickness relative to the core radius (10–12). Micellar crystallization into either an fcc or a bcc lattice is determined by the length scale and steepness of repulsive interactions that can be controlled by the ratio of the coronal layer thickness to the core radius (10). However, the implications of the unusual micellar structures of rod-coil block copolymers (6, 13) for regulating these repulsive interactions, micellar crystallization, and crystal lattice selection are yet to be investigated.

We report the self-organization of hollow

Departments of Chemical Engineering and Chemistry, University of Rochester, Rochester, NY 14627–0166, USA.

*To whom correspondence should be addressed. E-mail: jenekhe@che.rochester.edu